Naval Research Laboratory
Washington, DC 20375-5320

NRL/7320/MR—2021/6

An Alternative Representation of Frazil Ice in the NHWAVE Model

MARK D. ORZECH

Ocean Dynamics and Prediction Branch
Ocean Sciences Division

October 8, 2021

REPORT DOCUMENTATION PAGE

Form Approved
OMB No. 0704-0188

1. REPORT DATE *(DD-MM-YYYY)*	**2. REPORT TYPE**	**3. DATES COVERED** *(From - To)*
08-10-2021	NRL Memorandum Report	01 Oct 2020 – 30 Sep 2021

4. TITLE AND SUBTITLE

An Alternative Representation of Frazil Ice in the NHWAVE Model

5a. CONTRACT NUMBER

5b. GRANT NUMBER

5c. PROGRAM ELEMENT NUMBER

6. AUTHOR(S)

Mark D. Orzech

5d. PROJECT NUMBER

5e. TASK NUMBER

5f. WORK UNIT NUMBER
1R29

7. PERFORMING ORGANIZATION NAME(S) AND ADDRESS(ES)

Naval Research Laboratory
4555 Overlook Avenue, SW
Washington, DC 20375-5320

8. PERFORMING ORGANIZATION REPORT NUMBER

NRL/7320/MR--2021/6

9. SPONSORING / MONITORING AGENCY NAME(S) AND ADDRESS(ES)

Office of Naval Research
One Liberty Center
875 N. Randolph Street, Suite 1425
Arlington, VA 22203-1995

10. SPONSOR / MONITOR'S ACRONYM(S)

ONR

11. SPONSOR / MONITOR'S REPORT NUMBER(S)

12. DISTRIBUTION / AVAILABILITY STATEMENT

DISTRIBUTION STATEMENT A: Approved for public release; distribution is unlimited.

13. SUPPLEMENTARY NOTES

14. ABSTRACT

This report describes a series of phase-resolved simulations of small-scale interactions between waves and loosely aggregated, slushy sea ice commonly referred to as "frazil ice". The model NHWAVE (Ma et al., 2012) is employed to simulate waves in all cases. The model's routines for incorporating the damping effects of vegetation are modified to create a configurable representation of surface ice for a user-specified, fixed area of the water surface, while retaining the model parameters used for specifying the drag and blocking due to the vegetation. The frazil configuration parameters are varied to produce different degrees of wave damping for two different wave frequencies, and the effects on the free surface and the velocity profiles are examined and compared to theory. Several issues are identified with this new representation, and potential future improvements to resolve them are discussed.

15. SUBJECT TERMS

16. SECURITY CLASSIFICATION OF:			**17. LIMITATION OF ABSTRACT**	**18. NUMBER OF PAGES**	**19a. NAME OF RESPONSIBLE PERSON**
					Mark D. Orzech
a. REPORT	**b. ABSTRACT**	**c. THIS PAGE**	U	29	**19b. TELEPHONE NUMBER** *(include area code)*
U	U	U			(228) 688-5974

This page intentionally left blank.

NRL MEMORANDUM REPORT

An alternative representation of frazil ice in the NHWAVE model

Mark D. Orzech (NRL 7322)

Abstract:

This report describes a series of phase-resolved simulations of small-scale interactions between waves and loosely aggregated, slushy sea ice commonly referred to as “frazil ice”. The model NHWAVE (Ma et al., 2012) is employed to simulate waves in all cases. The model’s routines for incorporating the damping effects of vegetation are modified to create a configurable representation of surface ice for a user-specified, fixed area of the water surface, while retaining the model parameters used for specifying the drag and blocking due to the vegetation. The frazil configuration parameters are varied to produce different degrees of wave damping for two different wave frequencies, and the effects on the free surface and the velocity profiles are examined and compared to theory. Several issues are identified with this new representation, and potential future improvements to resolve them are discussed.

Contents

List of Figures

This page intentionally left blank.

1 INTRODUCTION

This report documents two series of numerical simulations of wave propagation through frazil ice. The simulations examine both wave attenuation and velocity profiles for a variety of cases in which waves propagate through frazil ice, with the first series using waves of period T=8s and the second series using waves with T=4s. These tests are intended to evaluate the performance of a modified version of the non-hydrostatic model NHWAVE, in which the model's vegetation damping parameterization is repurposed to represent damping by surface frazil. The modified NHWAVE is applied to simulate wave attenuation by frazil and investigate the associated profiles of horizontal and vertical velocity in and below the frazil layer.

The newly developed frazil configuration includes parameters allowing the user to adjust frazil thickness, density, permeability, drag coefficient, and virtual mass (in the form that these are provided for vegetation). While these parameters do not capture all physical aspects of actual frazil, they may be individually tuned to achieve a wide range of wave attenuation effects. However, some of the effects of the "veggie frazil" on the fluid behavior are of course not entirely realistic. Section 2 provides a brief description of the original model and the vegetation parameterization. Section 3 details the modifications made to NHWAVE to represent frazil ice. Section 4 presents results for a range of frazil configurations and two different wave periods and compares them to theory and field data, along with further discussion. Conclusions and plans are provided in Section 5, followed by references (Section 0) and suggestions for further reading (Section 7).

2 MODEL DESCRIPTION

The wave model used for all simulations in this study, NHWAVE, was developed at the University of Delaware, primarily by Gangfeng Ma, Jim Kirby, and Fenyan Shi. The model solves the incompressible Navier-Stokes equations in a 3D domain, after transforming the vertical dimension to a surface/bed following σ-coordinate. The transformed governing equations are written in the following conservative form:

$$\frac{\partial \Psi}{\partial t} + \nabla \cdot \Theta(\Psi) = S$$

where Ψ is the vector of conserved variables, Θ(Ψ) contains the flux variables, and

$$\nabla = \left(\frac{\partial}{\partial x}, \frac{\partial}{\partial y}, \frac{\partial}{\partial \sigma} \right)$$

On the right-hand side, S is a combined source term that includes separate components for bottom slope, pressure gradient, and turbulent mixing. Both Ψ and Θ are functions of water depth h, free surface η, and velocities u, v, and ω (the contravariant of the vertical velocity in the sigma dimension). Further details are provided in Ma et al. (2012), Derakhti et al. (2015), and Orzech et al., (2016).

Among other features, the model includes parameterizations for the wave-damping effects of vegetation growing up from the seabed. Users may specify either "rigid" or "flexible" vegetation in the model's input configuration file, but for the present study I am working with only the "rigid" vegetation option. Ma et al. (2013) implemented turbulence production by rigid

Manuscript approved October 7, 2021.

vegetation as a nonlinear k − ε model in NHWAVE, which they calibrated and validated using data from open channel flow and random wave propagation in vegetation fields. The authors found that the drag-related coefficients in the k − ε model C_{fk} and C_f could affect turbulent flow structure, but had less effect on wave attenuation in the surf zone.

The representation in NHWAVE of the flow field through rigid vegetation is described by the following equations (Ma et al., 2013):

$$\partial \langle \bar{u}_i \rangle / \partial x_i^* = 0$$

$$\partial \langle \bar{u}_i \rangle / \partial t^* + \langle \bar{u}_j \rangle \partial \langle \bar{u}_i \rangle / \partial x_j^* = -\frac{1}{\rho} \partial \langle \bar{p} \rangle / \partial x_i^* + g_i + \partial \tau_{ij} / \partial x_j^* + f_{Fi} + f_{Vi}$$

in which

$$\tau_{ij} = -\langle \overline{u_i' u_j'} \rangle - \langle \bar{u}_i'' \bar{u}_j'' \rangle + \nu \, \partial \langle \bar{u} \rangle / \partial x_j^*$$

$$f_{Fi} = 1/V \iint_{S_i} \bar{p} n_i dS$$

$$f_{Vi} = -\nu/V \iint_{S_i} \frac{\partial \bar{u}_i}{\partial n} dS$$

Above, x_i* represents the coordinates in the Cartesian frame of reference, u_i is the velocity components, ρ is water density, p is water pressure, and g_i is gravity (nonzero only in z-direction). The viscous drag and form drag of the vegetation, f_{Vi} and f_{Fi}, respectively, are modeled together as

$$f_{di} = f_{Vi} + f_{Fi} = C_D \lambda u_i |u| / 2$$

where C_D is a drag coefficient and $\lambda = b_v N$ is vegetation density, with b_v representing the stem size and N representing the number of stems per unit area. The inertial or "virtual mass" force is given by

$$f_{vmi} = \frac{C_M \pi b_v^2 N}{4} \frac{\partial u_i}{\partial t}$$

in which C_M is the virtual mass coefficient. These additional components are incorporated into NHWAVE's surface-and-bottom-following sigma coordinate system. For complete details on the formulation, see Ma et al. (2013).

Several parameters from among those mentioned above are provided to the user for configuring the vegetation effects in the input file for NHWAVE. These include vegetation density λ (VegDens, $1/m^2$), stem size b_v (VegBV, m), drag coefficient C_D (VegDrag, unitless), and virtual mass coefficient C_M (VegVM, unitless). Several other parameters are provided in the input file, but they were not utilized for this study. The parameter settings used in the calibration and

validation of this system by Ma et al. (2013) were, of course, restricted to those that might reasonably apply to actual vegetation. Also, those tests were limited to the nearshore, where wave attenuation by depth is significantly greater than it would be farther offshore. Here, the "rigid" vegetation parameterization is modified to represent frazil ice at the surface only and these parameters are allowed to vary more widely, as described in detail in Section 3 below.

3 IMPLEMENTATION OF "VEGGIE FRAZIL"

As noted above, this report describes simulations with a new representation of frazil ice based on the vegetation parameterization in NHWAVE. For convenience, I shall occasionally refer to this type of frazil as "veggie frazil". In this section, the modifications made to create this vegetation-based alternative frazil representation in the standalone NHWAVE model will be described, along with the associated test configurations.

For this study, a relatively simple set of modifications is applied to the "rigid" vegetation configuration of standalone NHWAVE to represent frazil ice in a fixed surface location. Through small changes to criteria for vegetation height (VegH) in the main program, the vegetation effects are limited to a layer near the water surface, whose thickness is specified by the user in the input file. With these modifications, the vegetation damping only acts on the fluid fluxes at depths that are less than the specified frazil thickness. For greater depths, the damping is not activated.

Unlike the validating studies described in Section 2, all simulations here are conducted in water of constant depth and parameters are allowed to vary much more greatly than would be expected for actual vegetation. The tests are run in 2D (x, z only), with vertical grid spacing of dz=0.1m (i.e., 150 vertical sigma levels) in 15m depth. The relatively high vertical resolution is used in order to see some of the model-estimated structure of the flow field in the boundary layer along the underside of the frazil. Two different series of simulations are run, utilizing a range of vegetation parameter configurations in combination with initial waves of either period T=8s or T=4s. The horizontal resolution is dx=1.0m for the 8s waves and dx=0.2m for the 4s waves. The moderate-to-high horizontal resolution is necessary in each case to reduce numerical dissipation of waves as they progress through the tank.

The vegetation parameter configurations for both sets of simulations are summarized in Table 1. They include one "max" configuration, in which all parameters are set to very large values, and one "min" configuration with all parameters set to nominally smaller values, as well as several "mixed" configurations, which are identical to the "max" configuration except that a single parameter is set to the "min" value. For six tests (#1 - #6) the frazil thickness is set to 1m, while for two additional tests (#1b and #6b) the frazil thickness is set to 3m.

Table 1. NHWAVE Frazil Configurations for Two Test Series

Test Case #	Test label	Density ($1/m^2$)	Stem Diameter (m)	Drag Coefficient	Virtual Mass Coefficient
1	lo	1250	0.001	0.10	0.1
2	mid1	1250	0.01	1.0	1.0
3	mid2	2250	0.001	1.0	1.0
4	mid3	2250	0.01	0.10	1.0
5	mid4	2250	0.01	1.0	0.1
6	hi	2250	0.01	1.0	1.0
7	***lo3m***	1250	0.001	0.10	0.1
8	***hi3m***	2250	0.01	1.0	1.0

As noted above and listed in Table 1, the newly configured frazil ice has a series of different parameters that may be used to change its permeability and drag. While these parameters were originally designed for vegetation, they are repurposed here to represent different aspects of the frazil. Specifically, the permeability of the frazil is represented via the "Stem Diameter" of the vegetation, the form drag of the frazil is implemented through the "Density" and "Virtual Mass" coefficients, and the shear drag of the frazil is configured through the "Drag Coefficient" of the vegetation.

For both of the test series, the attenuation in wave height is measured by tracking the vertical range of the water surface (1) at the front of the frazil edge and comparing it to the corresponding range (2) at a location inside the frazil, 100m beyond the front edge of the ice (see Figure 1). All simulations specified a monochromatic initial wave at the wavemaker. The first set of simulations used a wave height of 0.5m and a period of 8s (corresponding to a wavelength of ~100m), while the second set used a wave height of 0.2m with a period of 4s (~25m). The frazil was configured to extend vertically from the specified depth (VegH) to the surface. For both series, the value of VegH was set to 14m in tests #1 – 6 (i.e., frazil extended 1m below the still water level water surface), and it was set to 12m in tests #7 & 8 (i.e., 3m-thick frazil). Results are compared to expectations based on theory and field data.

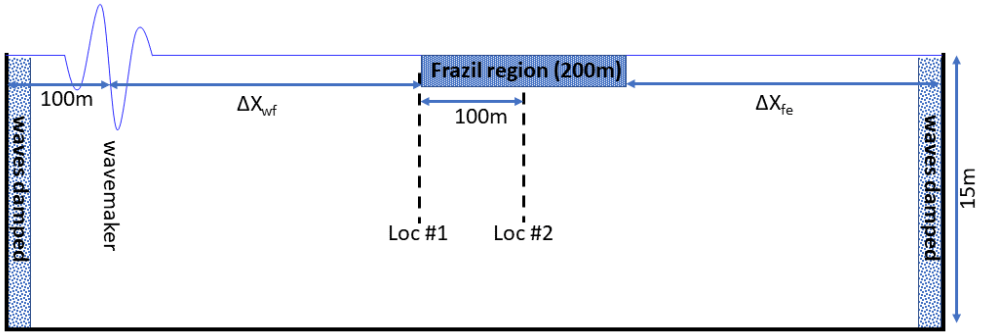

Figure 1. NHWAVE configuration for simulations of wave interaction with frazil ice region. The distance between wavemaker and frazil (ΔX_{wf}) is 300m for T=8s waves and 80m for T=4s waves (i.e., roughly 3 wavelengths for each series). The distance between frazil and end of tank (ΔX_{fe}) is 400m for T=8s waves and 52m for T=3s waves (The latter tank setup was shortened to reduce overall computation time for the T=3s simulations).

The vertical profiles and time series of horizontal velocity (u) and vertical velocity (w) are also extracted for locations in the vicinity of the frazil ice. The goals of this part of the analysis are to examine the phase shift between fluid flow in the ice in comparison to the flow underneath, to measure predicted properties of the boundary layer at the ice-water interface, and to understand how the profile, phase shift, and boundary layer are affected by different frazil ice configurations. These results are also compared with those expected from theory.

4 RESULTS

This section presents results from the numerical investigations described in Section 3. The wave attenuation results are described in Section 4.1. The model-predicted velocity profiles and time series for both horizontal and vertical velocities are detailed in Section 4.2. Further discussion is provided in Section 4.3, focusing in particular on the unusual results obtained along the ice-ocean boundary.

4.1 Wave Attenuation

The effects of different frazil types on wave attenuation for the two simulation series and eight test cases are illustrated with free surface cross sections in Figure 2 and Figure 3. As anticipated, the greatest attenuation is seen for the two "hi" resistance frazil cases (#6 and #8, shown as red solid and black dashed lines, respectively, in each figure). The 3m-thick, high resistance frazil causes considerably more attenuation than even the 1m-thick, high resistance frazil. The least attenuation is seen with both the "lo" resistance frazil cases (#1 and #7, shown as blue solid and black dashed lines, respectively). In contrast to the "hi" cases, however, the attenuation for the 1m-thick frazil appears to be essentially the same as for the 3m-thick frazil. While nearly all of the "mid" frazil cases (green dotted) produce attenuation levels between those of the 1m "hi" and the 1m "lo" frazil, one case (#4) actually produces more attenuation than the 1m "hi" frazil (This result is visible as a single green dotted line with amplitude slightly less than the red solid line).

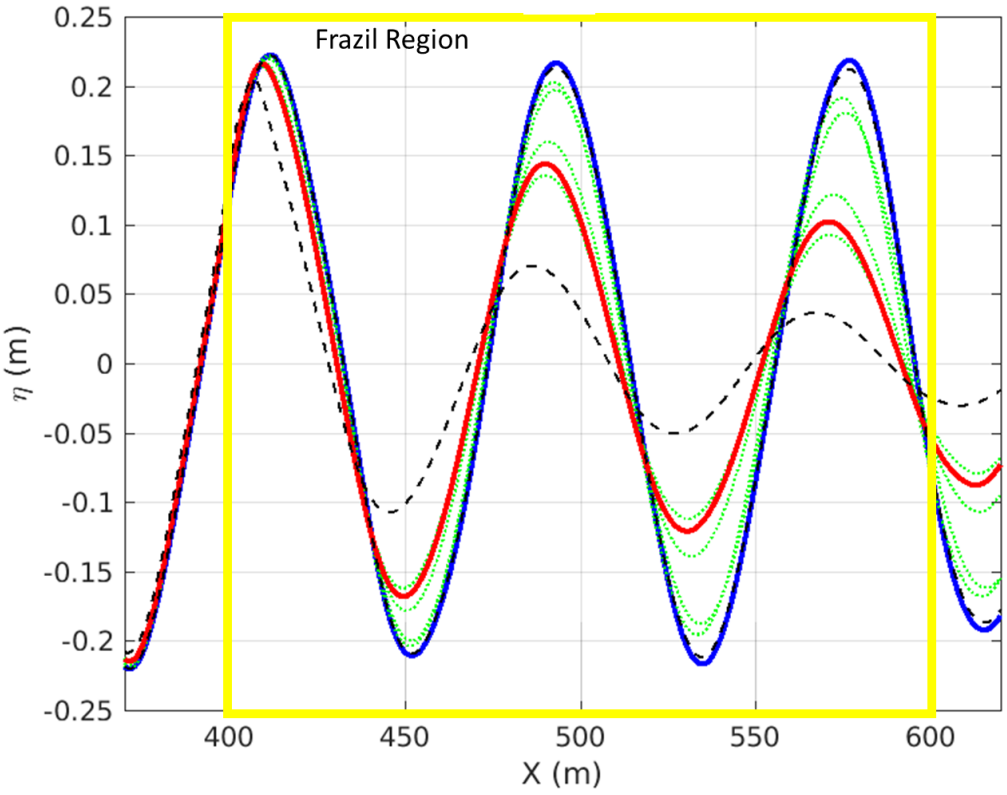

Figure 2. Comparison of surface elevations, η, for the eight tests summarized in Table 1, using wave period **T=8s**. All results are at model timestep t=90s. Test #1 ("lo") is solid blue, test #6 ("hi") is solid red, and both the "lo3m" and "hi3m" cases are plotted as black dashed lines. All other "mid*" cases are green dotted lines. The one "mid" case with dissipation slightly greater than the "hi" case is "mid4", in which a virtual mass of 0.1 was assigned (versus a value of 1.0 for the "hi" case).

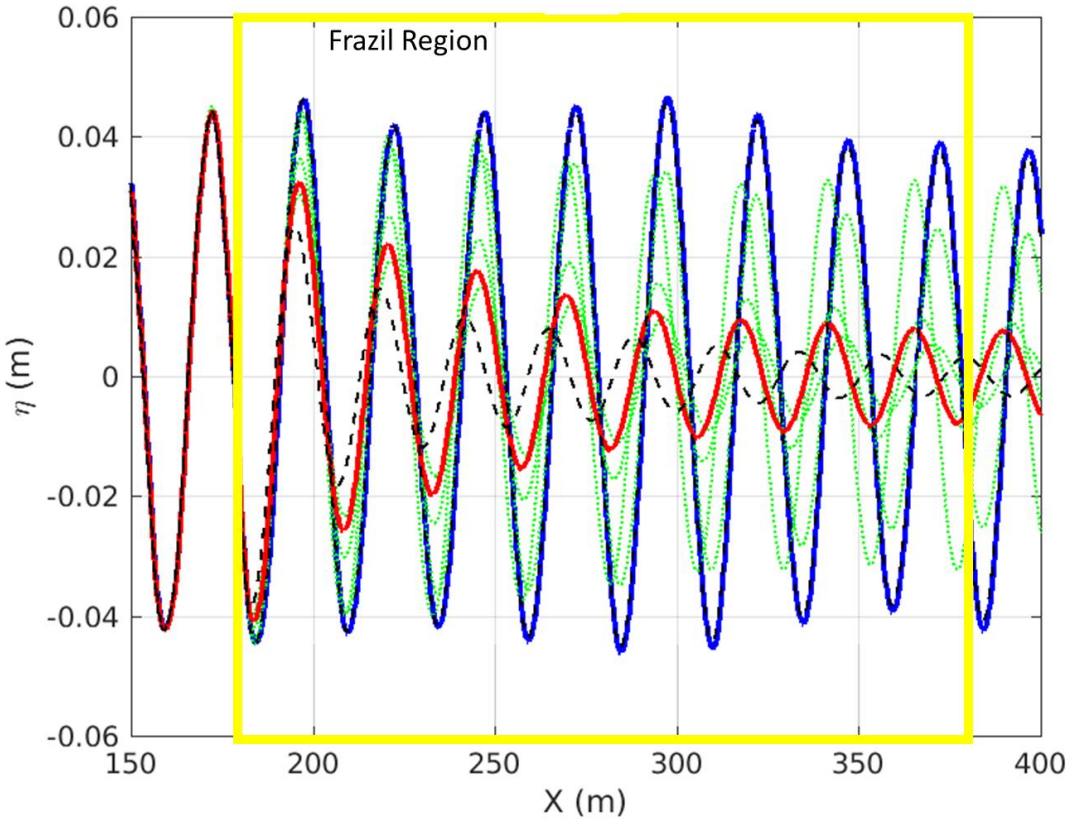

Figure 3. Comparison of surface elevations, η, for the eight tests summarized in Table 1, using wave period **T=4s**. Line colors are same as described in Figure 2. Note that frazil position is different from T=8s simulations, but frazil length (200m) remains the same.

An alternate view of the attenuation is presented in Figure 4 and Figure 5, in which the standard deviations of the free surface oscillation are measured and compared at two locations, one at the front end of the frazil ice and another 100m inside the frazil (i.e., Loc #1 and #2 in Figure 1, respectively). The total height of each combined bar corresponds to the standard deviation of the free surface at the front of the frazil (measured over 40 seconds), while the height of the blue portion of each bar corresponds to the same standard deviation measured after propagating 100m into the frazil.

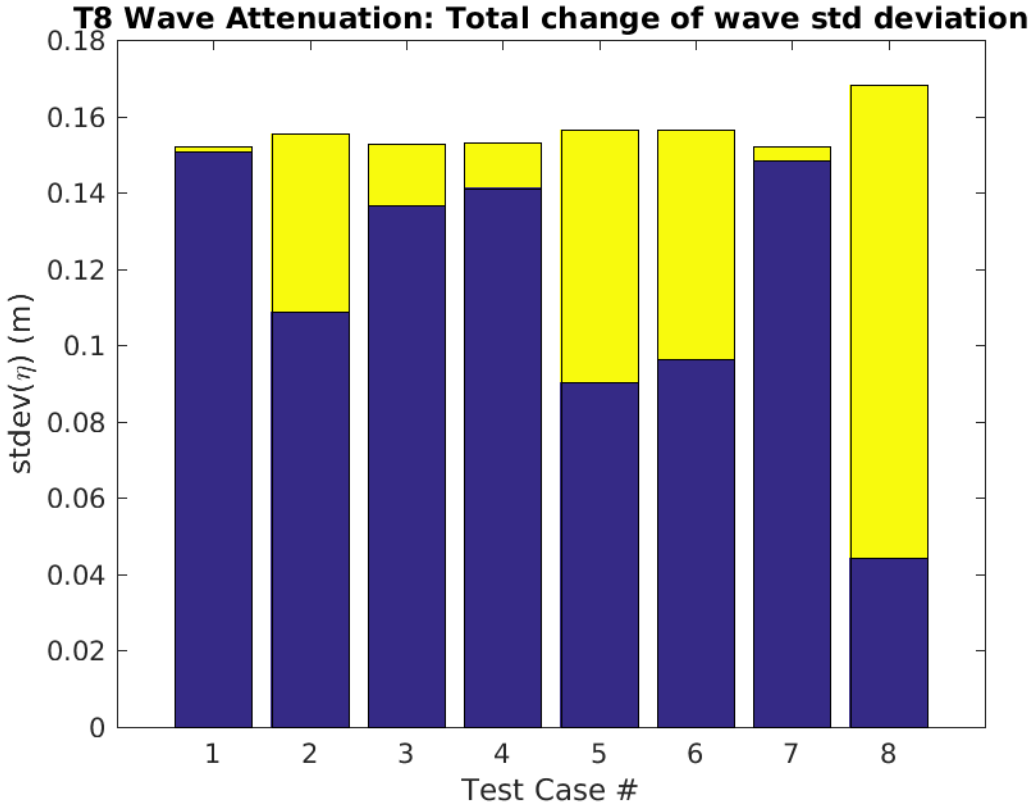

Figure 4. Change in standard deviation of free surface for the eight frazil test cases listed in Table 1, for initial wave period **T=8s**. Total height of each bar corresponds to standard deviation of free surface at a location directly in front of the frazil (x = 400m). Height of blue portion of each bar corresponds to standard deviation of free surface at location 100m past the frazil front edge (x = 500m). Yellow portion of each bar thus illustrates total wave attenuation between the two locations. Standard deviations are calculated between t=80s and t=120s (approximately 5 wave periods).

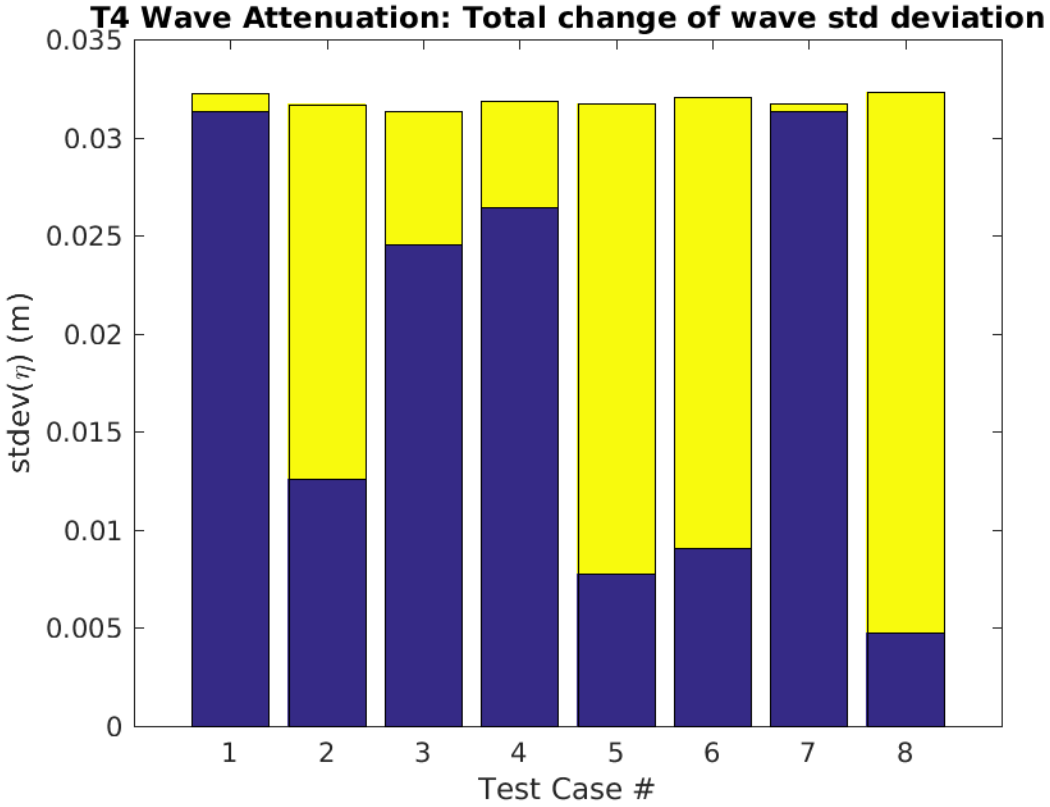

Figure 5. Change in standard deviation of free surface for the eight frazil test cases listed in Table 1, for initial wave period **T=4s**. Same configuration as Figure 3, except that in this case the frazil itself and each of the two measurement locations have moved 120m closer to the wavemaker. Standard deviations are again calculated between t=80s and t=120s (approximately 10 wave periods).

However, the attenuation shown in Figure 2 through Figure 5 does not represent only wave attenuation due to frazil effects. It also includes a small amount of wave attenuation due to numerical dissipation. This artificial dissipation has been reduced to just a negligible fraction of overall dissipation by using a relatively high horizontal resolution (dx=1m and 0.2m respectively, as noted earlier) and does not noticeably affect the results of Figure 4 or Figure 5.

The attenuation results are now used to estimate damping coefficients, k_i, following the standard theoretical prescription

$$H(\Delta x) = H_o e^{-k_i \Delta x}$$

which may be rewritten as

$$k_i = \frac{1}{\Delta x} \cdot \ln\left(\frac{H_o}{H(\Delta x)}\right)$$

In these expressions, H_o is initial wave height, $H(\Delta x)$ is final wave height, and Δx = 100m. The k_i values are shown for the eight test cases and both wave period values in Figure 6, and they range from 8.5e-5 to 2.5e-2. The damping coefficients for period T=4s range from 2.0e-4 to 2.5e-2, while those for period T=8s are consistently lower, ranging from 8.5e-5 to 1.5e-2. In comparison, results estimated from field data by Rogers et al. (2016) indicate a range of roughly 2.0e-6 to 2.0e-5 for varied distributions of frazil and pancakes that were observed during the 2015 Sea State Arctic experiment. This suggests that even the "lo" the parameters selected for

frazil in these simulations may need to be reduced considerably to more accurately reproduce effects seen in the field.

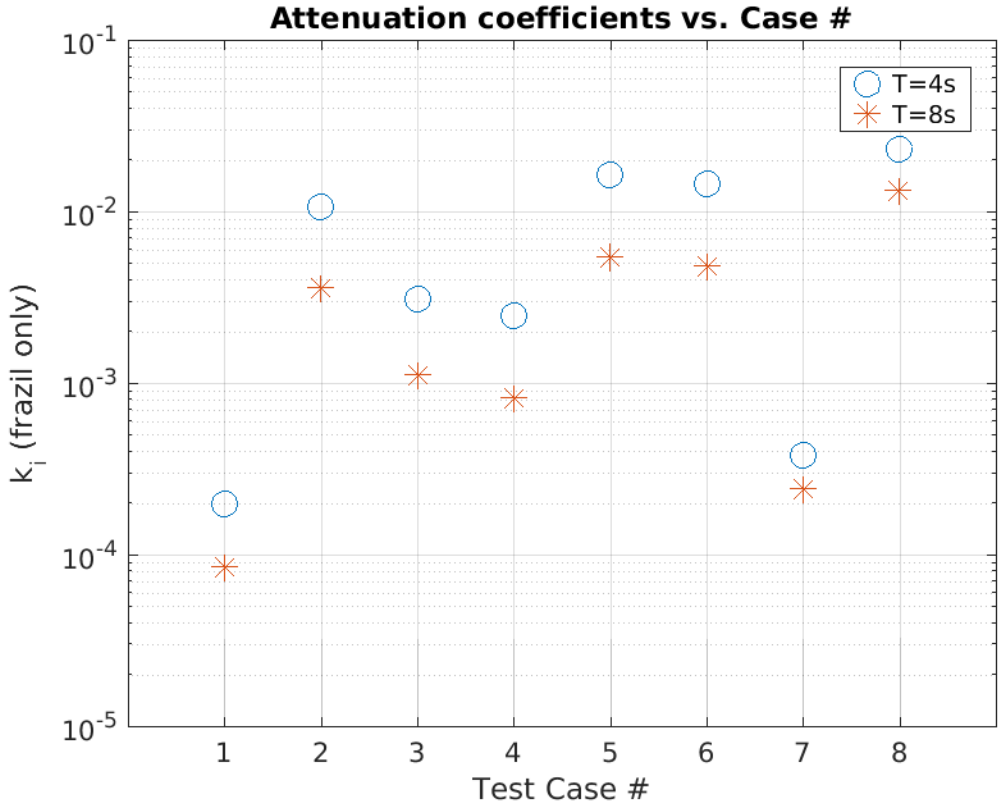

Figure 6. Estimated damping coefficients for the eight frazil ice configurations in Table 1, for wave periods T=8s (asterisks) and T=4s (circles).

4.2 Velocity Profiles and Time Series

4.2.1 Horizontal velocities

Model-estimated profiles of horizontal velocity for the T=8s simulations are shown under a wave crest and a wave trough in Figure 7 and Figure 8, respectively, including each of the 8 test cases of Table 1 (The T=4s profiles are similar and will not be included here). As expected, there is a clear discontinuity between the damped velocity in the ice region (i.e., z>14m in first six panels, z>12m in final two panels) and the velocity in the ice-free water beneath.

Negative Velocity Spike

Somewhat surprisingly, there is also a consistent negative "spike" in velocity at a depth just below the bottom of the frazil (seen in both the T=8s and T=4s output, though less exaggerated in the T=4s results). This spike occurs in all test cases and always produces a negative shift in horizontal velocity, whether under a crest or under a trough. It is larger for all six "hi" and "mid*" cases but almost disappears for the two "lo" cases. It seems likely that this spike is generated by the model to correct for the imbalances in fluid flux through the frazil versus fluxes through the ice-free region. However, it is likely not an accurate representation of a return flux that might be found under such conditions in the lab or field.

Note also that the negative spikes in Figure 7 and Figure 8 appear to be smaller for the "3m" cases in which the frazil is thicker. This seems contrary to what might be expected, as a thicker frazil barrier would be expected to block a greater amount of fluid flux, resulting in even greater fluid imbalances before and after the frazil region. However, because the velocity magnitude decreases with depth, it may be that this leads to a smaller overall difference in flux between the larger, damped frazil region and the lower-but-slower region underneath.

The negative-directed fluid flux runs along the entire base of the frazil ice, as illustrated by the two-dimensional x-z cross section of the T=8s horizontal velocity in Figure 9. The magnitude of this negative-directed flow is greatest near the front end of the frazil and gradually tapers off for locations closer to the downwave end. The flow actually becomes slightly positive-directed in a small region at the downwave end, just before reaching open water.

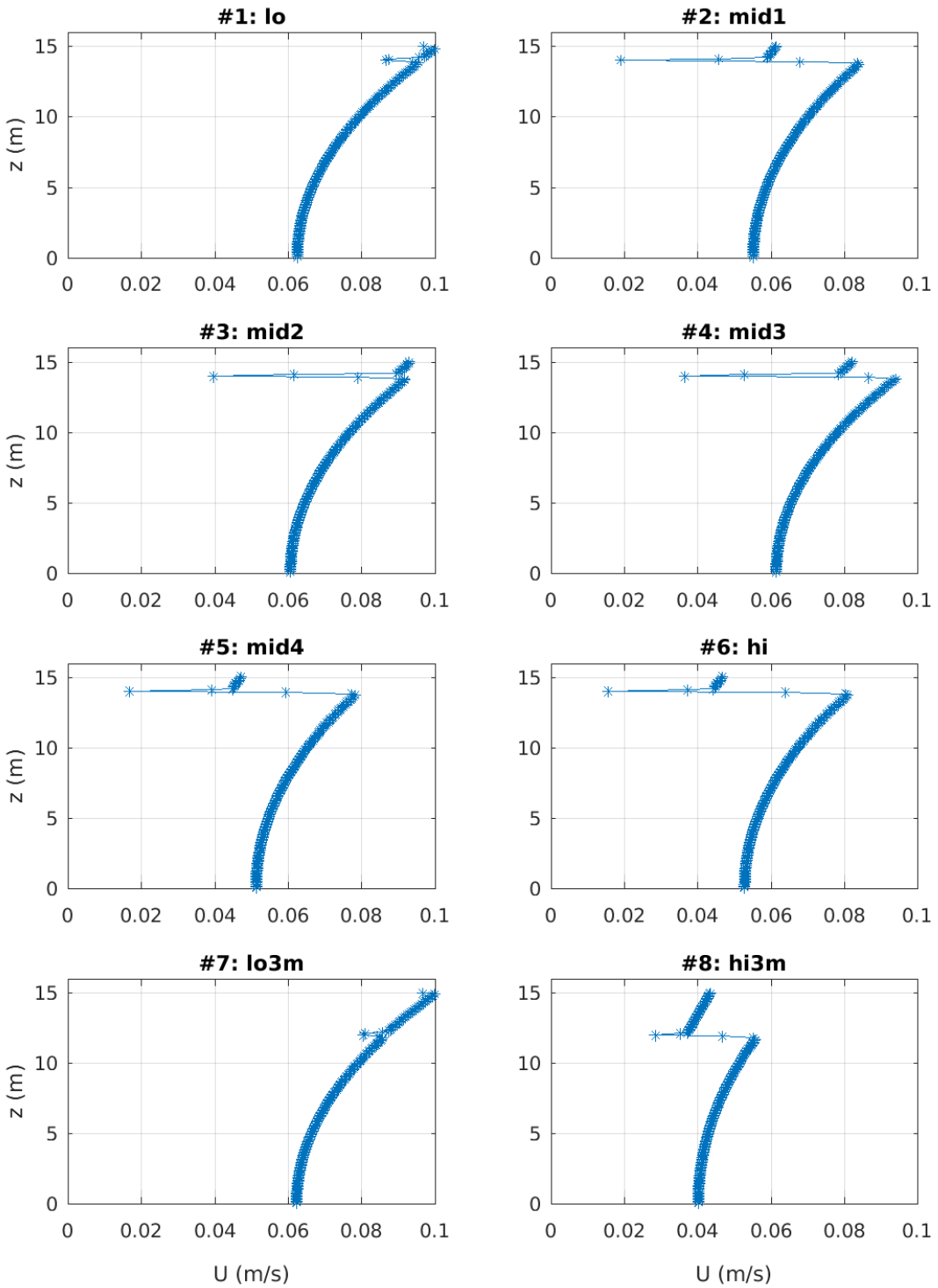

Figure 7. Profiles of horizontal velocity at tank location x=450m (i.e., 50m past the beginning of the frazil ice). At this timestep (t=120s), a wave **crest** is passing through this frazil location. Panel numbers correspond to the test numbers in Table 1. Note that frazil is 1m thick for top six panels and 3m thick for bottom two panels.

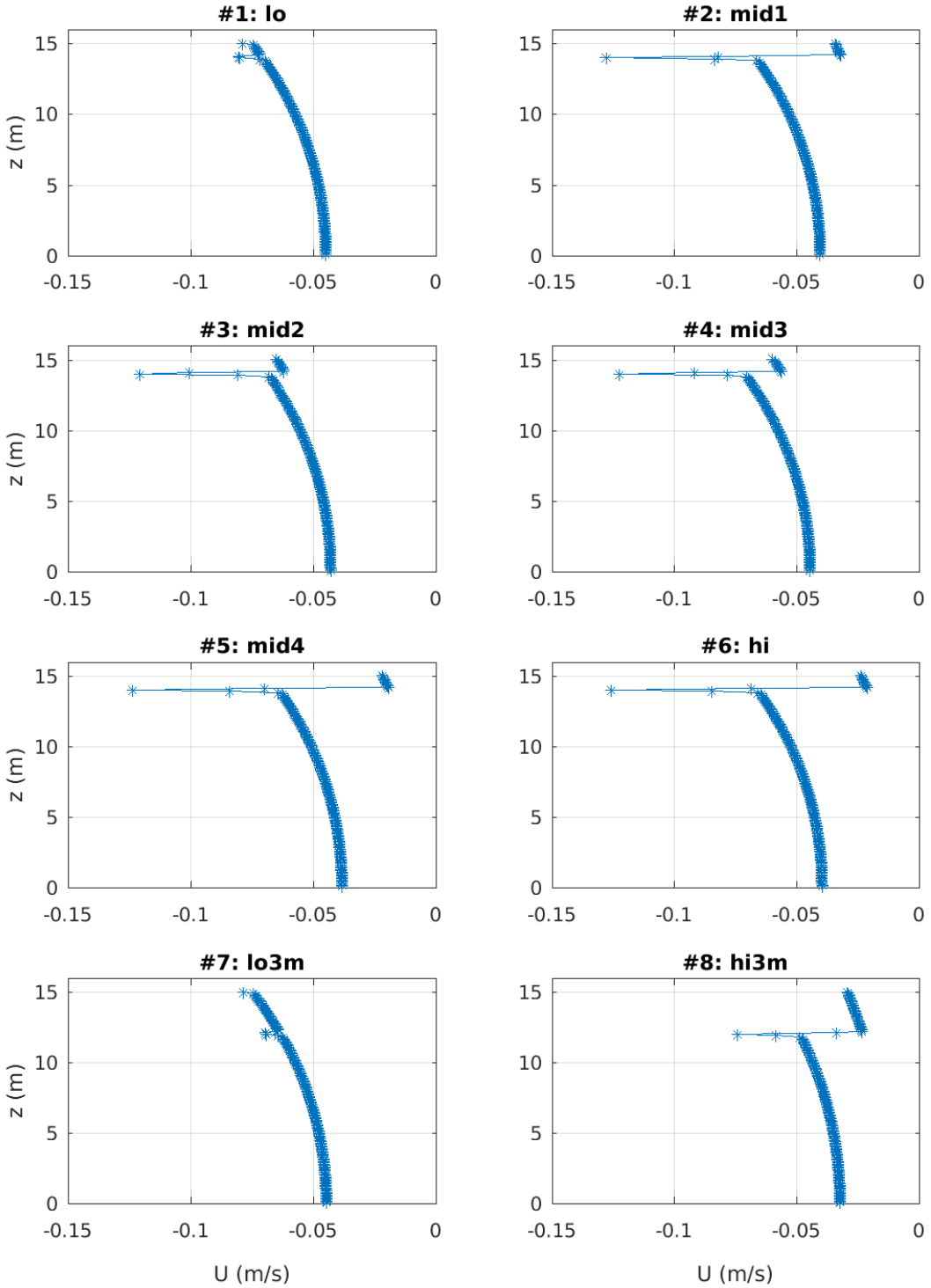

Figure 8. Profiles of horizontal velocity at tank location x=450m (i.e., 50m past the beginning of the frazil ice). At this timestep (t=115s), a wave **trough** is passing through this frazil location. Panel numbers correspond to the test numbers in Table 1. Note that frazil is 1m thick for top six panels and 3m thick for bottom two panels.

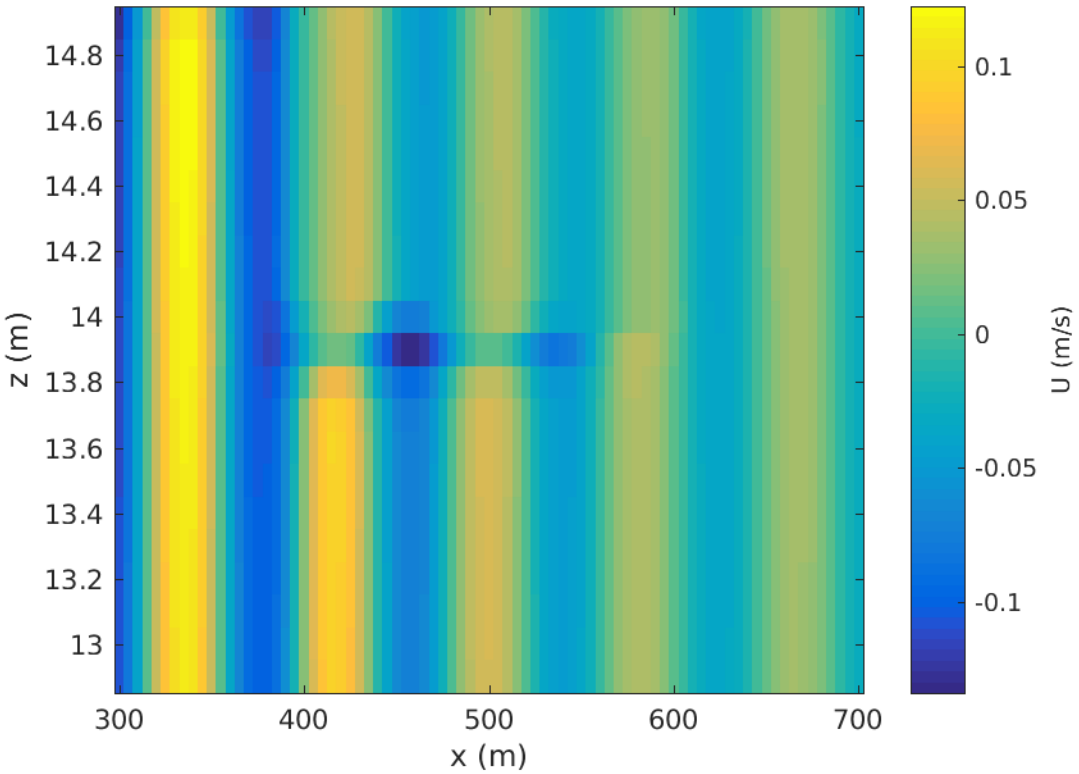

Figure 9. Horizontal velocity field versus depth for along tank cross-section extending from 2m depth (z=13m) to surface (z=15m) and x=300-700m alongshore. Result is from T=8s, case #6 ("hi"), with high density, 1m-thick frazil. Frazil region in this plot runs from z=14-15m and x=400-600m. Negatively directed spike in velocity is visible primarily at z=13.9m, just under frazil, and extends for entire alongshore length of frazil (becoming weaker for greater x and then slightly positively directed near x=600m).

The effects of the negative-directed velocity spike on relative horizontal velocity vary with alongshore location in the tank (as shown for T=8s waves in Figure 10), but they are again consistently greater in the frazil region (x=400-600m) for test cases in which the frazil is configured to have greater resistance ("hi*" and "mid*" cases) and negligible for cases with minimal resistance ("lo*" cases). Examining just the difference between the velocity in the frazil and the velocity below the frazil (at 10m depth) for the T=8s waves, I again find that there is essentially no effect for the "lo*" configurations but a consistently measurable effect in all other cases (Figure 11).

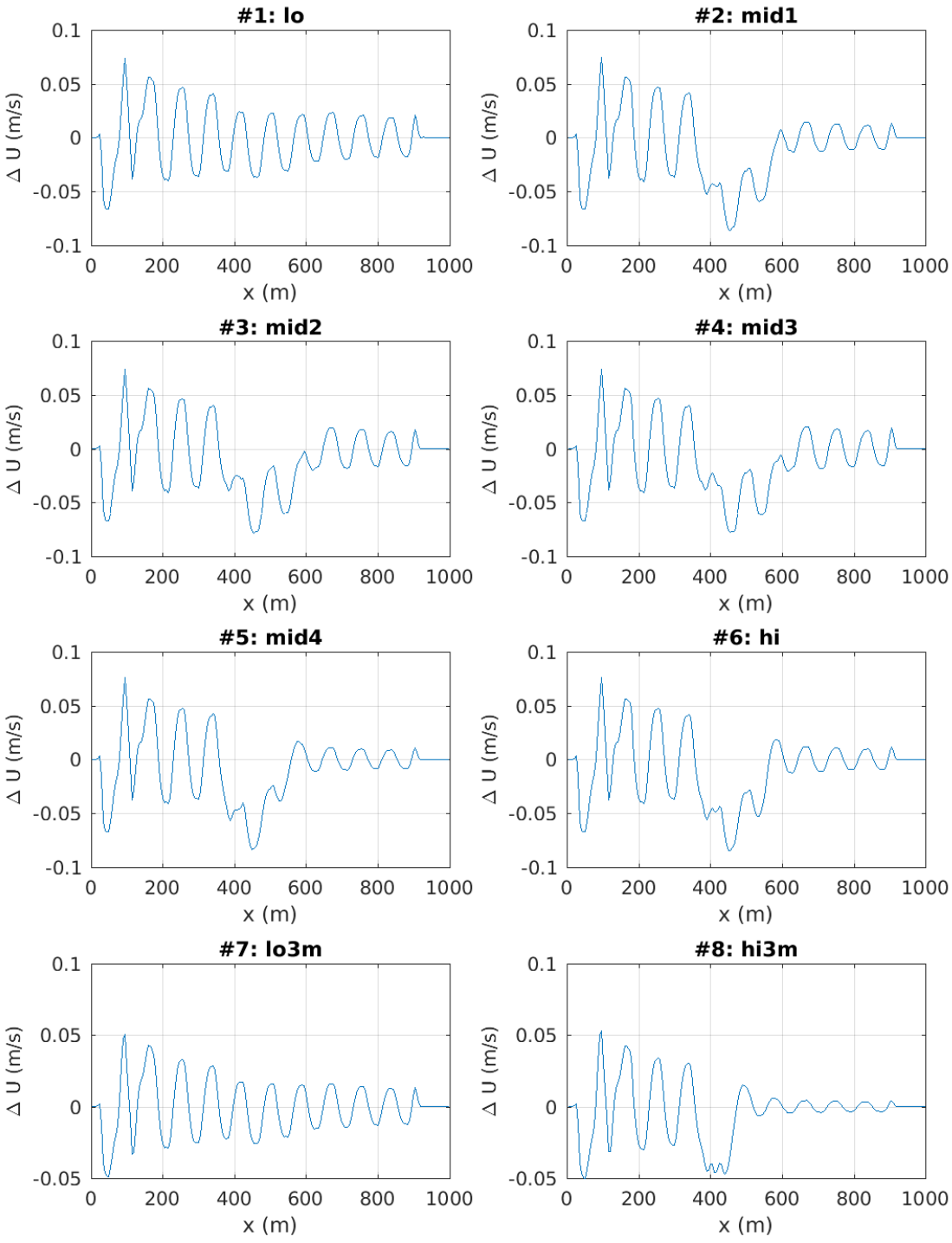

Figure 10. Difference of horizontal velocity at all locations along the tank for T=8s waves (same time as Figure 8). Velocity difference ΔU is computed as $\mathbf{U_{subfraz} - U_{10m}}$, where $U_{subfraz}$ is velocity at depth ***just below the underside of the frazil*** (i.e., z = 14m for panels #1-6 and z = 12m for panels #7-8), and U_{10m} is velocity at z = 10m. Frazil is located between x = 400-600m.

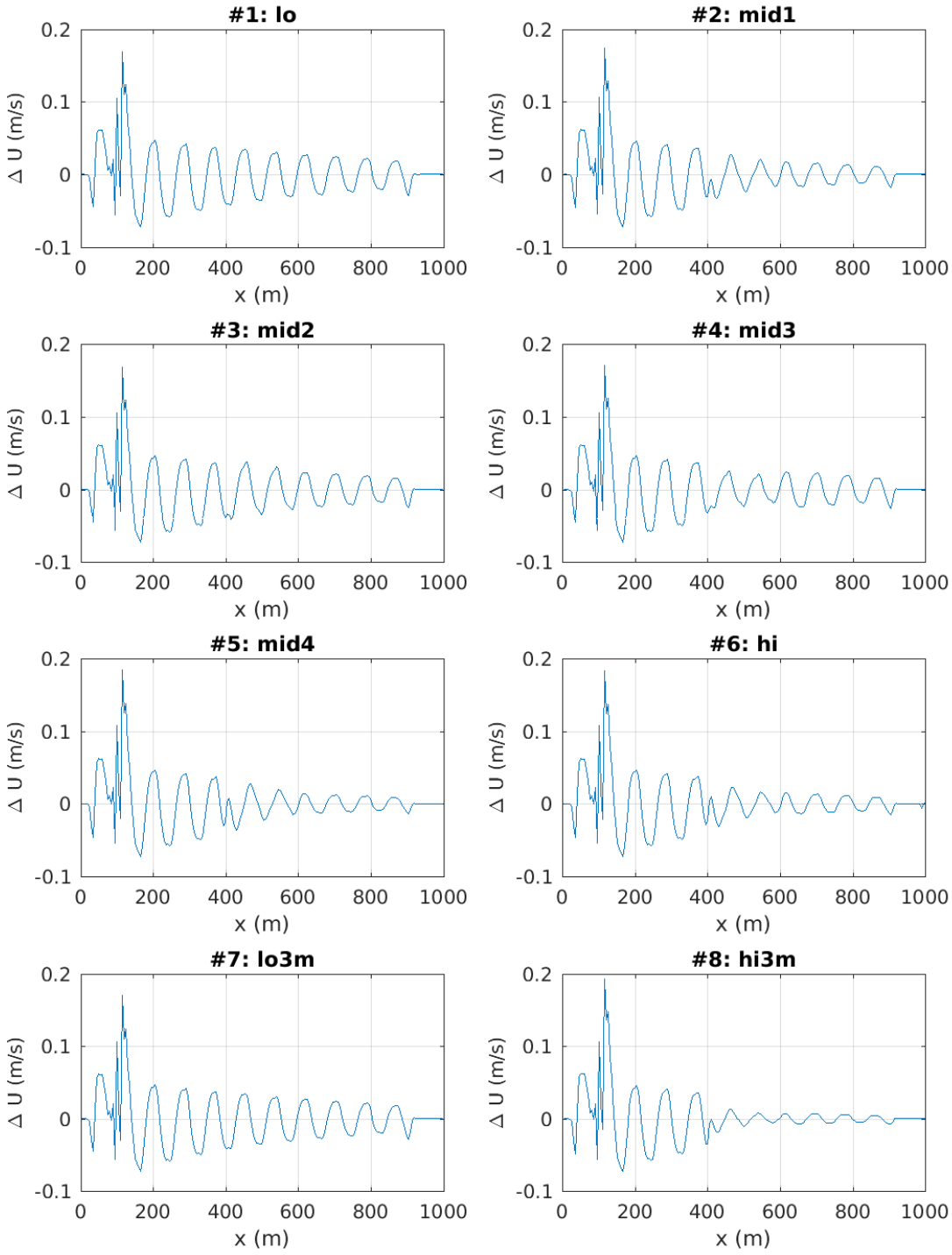

Figure 11. Difference of horizontal velocity at all locations along the tank for T=8s waves (same time as Figure 7). Velocity difference ΔU is computed as $\mathbf{U_{fraz} - U_{10m}}$, where U_{fraz} is velocity at depth ***in frazil just below the water surface*** (i.e., z = 14.9m for all panels), and U_{10m} is velocity at z = 10m. Frazil is located between x = 400-600m.

Phase Differences in Horizontal Velocities

The phase difference between horizontal velocity in the frazil and beneath is small in most cases, but there are several results for T=8s waves in which this difference is unexpectedly large (Figure 12). In these results, the greatest phase differences are recorded for the "mid1", "mid4" and "hi" cases (#2, #5 and #6), corresponding to approximately 0.8 seconds (or a phase shift of 36˚ out of 360˚). There are also moderate phase differences of 0.4 seconds (18˚) in three other cases (#3, #4, and #8). The two "lo" density frazil cases (#1 and #7) both exhibit zero phase difference.

The figure also displays a strange irregularity in several of the velocity time series for the clear water beneath the ice (e.g., cases #4 and #6), in which the time series departs considerably from its expected sinusoidal profile. The velocity time series for all panels of this figure were recorded at a depth of 5m, which was believed to be unaffected by the velocity "spikes" discussed earlier in this section. However, these irregular results for the T=8s waves suggest that may not have been true.

In the results for the T=4s waves (Figure 13), the phase differences are consistently near zero, with the greatest differences, only 0.2 seconds (or a phase shift of 18˚ out of 360˚), recorded for the "lo" and "lo3m" cases (#1 and #7). This non-zero shift corresponds to a single model time step, and is likely due to small resolution-related model output differences. This result is in accordance with wave theory, which predicts only a change in wavelength for waves propagating through surface ice and not a change in frequency.

The clear contrast in the phase shifts seen with the T=8s waves and will be addressed further in the Discussion below (Section 4.3).

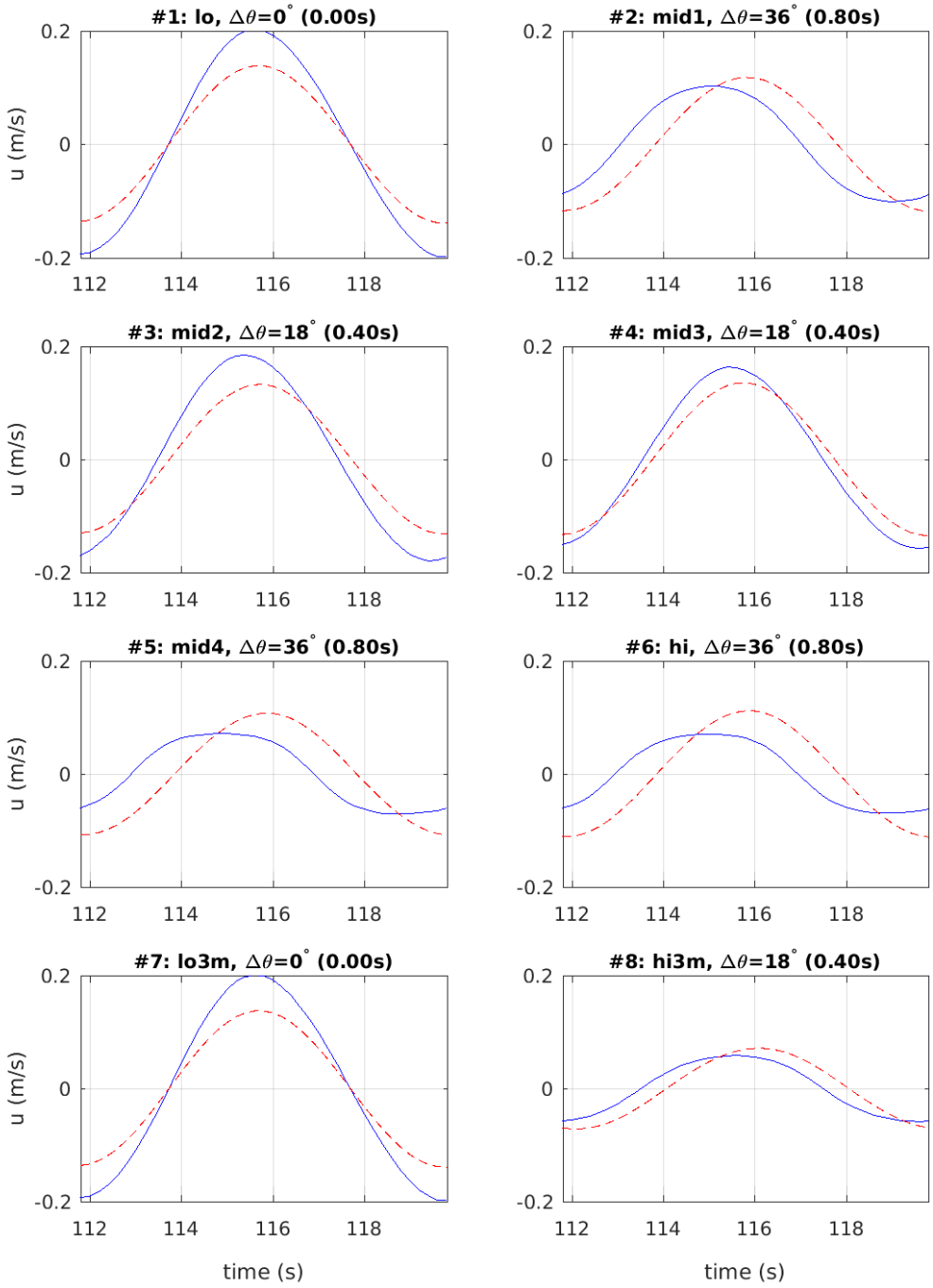

Figure 12. Along-tank (U) velocity time series (**T=8s** waves) measured at a horizontal location 50m past the frazil front edge, at vertical locations 0.5m below the frazil surface (blue solid) and at a depth of 5m below the surface (red dashed). Results shown are for all 8 test cases as described in Table 1. Phase differences Δθ are determined in each panel by identifying the time of the peak for the two measurement locations and comparing them. Greatest phase shifts (Δt = 0.8s) occur for moderately-to-highly damped cases #2, 5, and 6.

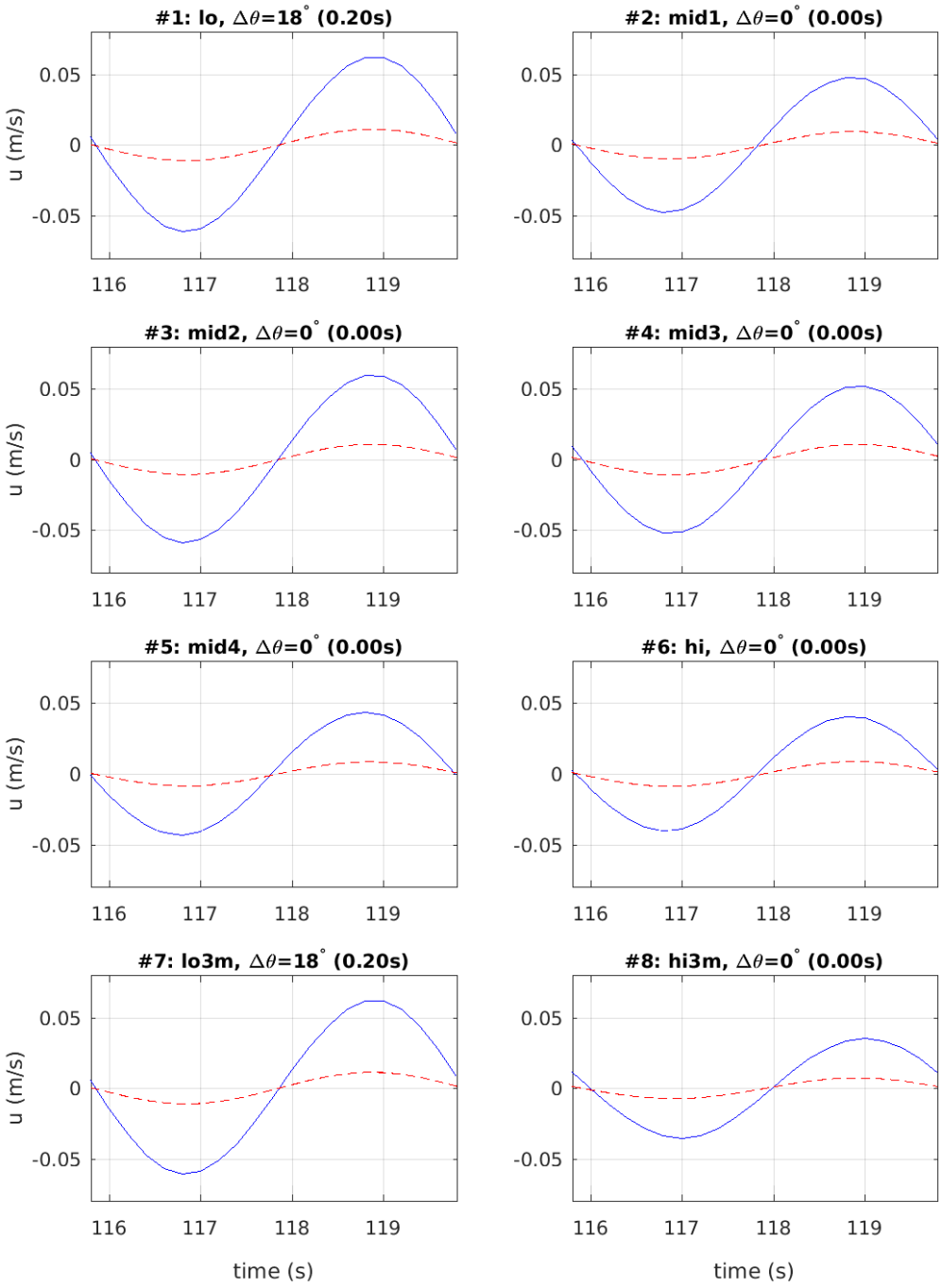

Figure 13. Along-tank (U) velocity time series (**T=4s** waves) measured at a horizontal location 50m past the frazil front edge, at vertical locations 0.5m below the frazil surface (blue solid) and at a depth of 5m below the surface (red dashed). Otherwise same configuration as Figure 12. Phase shifts in this case are consistently near zero, with just small nonzero values in cases #1 and #7 (Non-zero phase shifts of 9˚ or 0.2s correspond to one model timestep, dt=0.2s, and likely result from small numerical uncertainties).

4.2.2 Vertical velocities

As would be expected from theory, the frazil has a negligible effect on the phase of vertical velocity in the frazil region (Figure 14 and Figure 15). The phase difference is essentially zero for all 8 frazil configurations and both wave periods (with small non-zero results in cases #2, #5, and #8 likely resulting from model uncertainties).

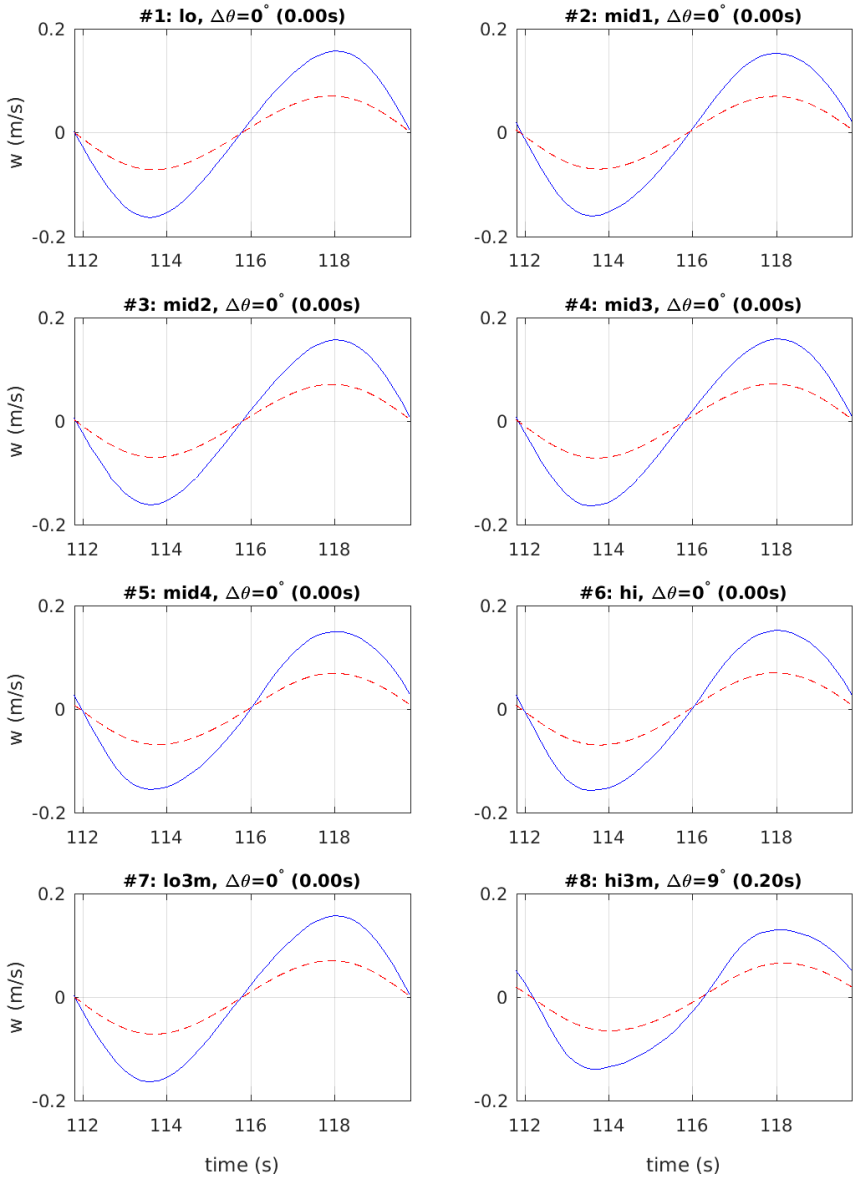

Figure 14. Vertical (W) velocity time series (for **T=8s** waves) measured at a horizontal location 50m past the frazil edge, at vertical locations 0.5m below the frazil surface (blue solid) and at a depth of 5m below the surface (red dashed). Results shown are for all 8 test cases as described in Table 1. Phase shift is again essentially negligible in all cases (within model uncertainty).

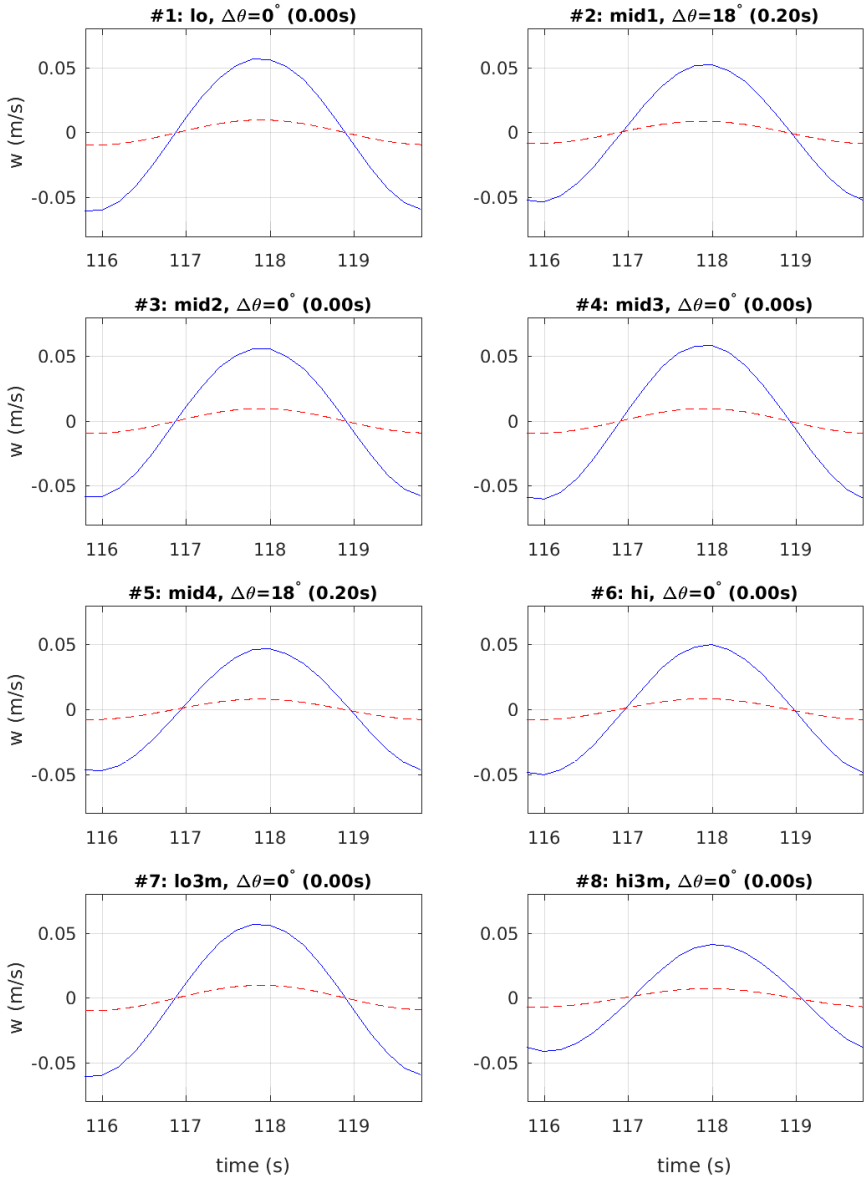

Figure 15. Vertical (W) velocity time series (for **T=4s** waves) measured at a horizontal location 50m past the frazil front edge, at vertical locations 0.5m below the frazil surface (blue solid) and at a depth of 5m below the surface (red dashed). Otherwise same configuration as Figure 14. Phase shift is once again essentially negligible in all cases.

4.2.3 Water-ice boundary layer

As noted in Section 3, the vertical grid spacing in these simulations was set to a fairly high resolution with the aim of capturing some of the vertical variations of the velocity profile in the boundary region itself. Figure 7 – Figure 9 give evidence that this boundary layer variation was captured for regions ranging from 10 – 50cm in thickness. The results were not what I had initially anticipated, because of the negatively directed fluxes discussed in Section 4.2.1 above.

Because of the negative spikes, it is not possible at this point to use these results to better understand the water-ice boundary layer in the ocean. This type of analysis could be further advanced if high resolution measurements of the flow field in this region were obtained in lab and/or field environments.

4.3 Discussion

The use of a rigid vegetation parameterization to represent the effects of flexible, mobile, surface frazil ice has numerous shortcomings. However, to the extent that a given region of frazil ice is roughly fixed in its location, it does appear that this approach can be tuned to produce wave damping and velocity profiles that are reasonably similar to those found in the field.

In Section 4.1, the parameters that I tested generally gave attenuation rates higher than those estimated for frazil and pancakes from field data by Rogers et al. (2016). However, the system proved to be highly tunable and responded consistently to reductions in parameters by producing a reduced attenuation rate. In these tests, the lowest wave attenuation for the parameter settings in Table 1 was obtained for case #1 ("lo") and the T=8s waves. The associated rate, k_i = 8.5e-5, was still about four times higher than the highest attenuation values seen in the field data. With respect to wave periods, the attenuation results are qualitatively consistent with those predicted by theory, with greater attenuation for T=4s waves than for T=8s waves in all cases.

The surface elevation snapshots shown in Figure 2 and Figure 3 also depict a gradual decrease in wavelength for all cases, with the greatest decreases occurring for T=4s waves in the more highly resistant ice (Figure 3, "hi" and "hi3m" cases). These results differ from what would be expected based on the theory of wave propagation in a viscous ice layer. In such a case, theory suggests that waves of period T=8s (f = 0.125Hz) and T=4s (f = 0.25Hz) should maintain an essentially constant wavelength (constant wavenumber k_r) relative to open water when they propagate through a typical viscous ice layer (Yu et al., 2019; see Fig 2a and 4a). However, it should be noted that the frazil ice used in this study may not have fit into the category of "typical" viscous ice. As noted above, attenuation results for all cases in Table 1were greater than those estimated by Rogers et al. (2016) for actual frazil and pancakes. Thicknesses used here may also have been greater than normally seen for frazil ice (especially in the 3m cases). Thus it is also possible that the somewhat extreme configuration of these tests may have produced non-physical effects of both excessive attenuation, wavelength reduction, and phase shifting in some of the cases. In contrast, waves of period T=4s (ω = 1.56rad/s) should see a significant increase in length.

Comparing the results for specific settings of the 8 cases from Table 1, it is clear that, as expected, the "lo" settings (cases #1 and #7) generally resulted in less attenuation than the remaining "mid" and "hi" cases, as would be expected. Looking at individual "mid" cases reveals a bit more about the effects of individual parameters. In particular, while applying a "lo" value for density, stem diameter, or drag coefficient (cases #2 - #4) did significantly increase wave attenuation relative to the original "hi" case (#6), reducing the virtual mass coefficient by an order of magnitude (case #5, "mid4") did not appear to affect the waves very much. In fact, the "mid4" and "hi" results are very similar for all comparisons shown in the figures above. As displayed in Figure 2 through Figure 6, the "mid4" case actually produced slightly more wave attenuation than the "hi" case, despite a lower value for virtual mass. It is not entirely clear why this happened; further study of the NHWAVE code itself will be needed to resolve this anomaly.

As the present study was principally aimed only at testing the feasibility and examining the peculiarities of this adapted system, I will not determine specific parameters for attenuation by "real frazil ice" at this time. This will be reserved for a future study. However, as a proof of concept, I did run one additional simulation employing much lower values of the Table 1 parameters than had been previously used (i.e., Density = 125 m^{-2}, Stem Diameter = 0.0001m,

Drag Coefficient = 0.01, Virtual Mass Coefficient = 0.01). This resulted in a wave attenuation rate of k_i = 9e-8, considerably lower than the lowest rate estimated by Rogers et al. (2016). The additional test also resulted in only negligible changes in wavelength and phase velocity in the lower viscosity ice layer. With additional tuning, the adapted wave model is thus clearly capable of capturing the attenuation ranges needed to simulate wave propagation through frazil ice, pancakes, and likely even larger ice floes (although permeability might ultimately become an issue for densely packed floes).

In Section 4.2.1, I highlighted the appearance of a seemingly anomalous negative-directed velocity spike in horizontal velocity profiles. It seems unlikely that such an effect would be encountered in the field, as it is likely produced by a setup imbalance in the wave tank resulting from Stokes transport by the wave crests. However, such a negative flux, possibly a counterflow balancing the effects of Stokes transport, may well exist and be measurable in a lab wave tank. This, too, will require additional investigation beyond the scope of the present study.

With additional simulations, I was able to considerably reduce the magnitude of the horizontal velocity profile spike by leaving a 20cm vertical gap of open water between the top of the frazil and the water surface in the model (i.e., the 1m-thick frazil that originally stretched from 1m depth to the surface instead was limited to depths between 20cm and 1m. This alteration resulted in a much larger spike in the horizontal velocity profile at the surface (which could be either positive, negative, or both simultaneously) and considerably reduced the size of the negative spike beneath the frazil. In Section 4.2.2, I found that the unusual spiking behavior in horizontal velocities did not show up in the vertically directed flow, which seemed to behave largely as expected.

5 CONCLUSIONS AND PLANS

As described above, I modified the vegetation parameterization in the non-hydrostatic wave model NHWAVE for use in approximating the effects of surface frazil ice. I found that the new configuration is very tunable and can be configured to produce widely varying levels of wave attenuation. I was able to use the modified code to produce wave attenuation similar to that measured in a field experiment (though of slightly greater magnitude).

When profiles of horizontal velocity were examined, this setup was found to consistently produce an unexpected, negatively-directed velocity "spike" (i.e., a narrowly focused flux oriented toward the negative x-direction) directly under the frazil ice layer. The spike became apparent as soon as the first wave had progressed over the frazil. It appears that this spike may be generated by the model's attempt to balance out the surface Stokes transport by the waves; however, I have not yet fully verified this explanation.

5.1 Possible improvements to frazil from vegetation

The present configuration of the "veggie frazil" representation in NHWAVE does not account for wave overtopping of the frazil. The frazil extends from the user-specified depth to the water surface, regardless of the amplitude of any waves passing through it. Thus all parts of passing waves that are above the bottom of the frazil will be damped. This might be made more realistic by configuring the frazil damping to extend only from the user-specified depth to the still-water level (i.e., the water surface in a quiescent tank). This would tend to reduce wave damping

somewhat, which may be more closely comparable to conditions in lab or field, particularly when waves overtop more consolidated areas of frazil ice.

5.2 Dissemination of Code

NHWAVE is presently considered an open-source, "community" model. Once security clearance has been obtained for public distribution, this modified version of the model will be provided upon request to scientists for non-commercial use, with the caveat that I am not responsible for errors in its output.

6 REFERENCES

Derakhti, M., J. T. Kirby, F. Shi, and G.Ma, 2015: NHWAVE: Model revisions and tests of wave breaking in shallow and deep water. University of Delaware Center for Applied Coastal Research, *Research Rep. CACR-15-18*, 127 pp.

Liu, A. K., B. Holt, and P. W. Vachon, 1991: Wave propagation in the marginal ice zone: model predictions and comparisons with buoy and synthetic aperture radar data, *J. Geophys. Res*., 96(C3), 4,605–4,621.

Ma, G., F. Shi, and J.T. Kirby, 2012: Shock-capturing non-hydrostatic model for fully dispersive surface wave processes. *Ocean Model.*, 43–44, 22–35.

Ma, G., J.T. Kirby, S.-F. Su, J. Figlus, & F. Shi, 2013: Numerical study of turbulence and wave damping induced by vegetation canopies. *Coastal Engrg*., 80, 68-78.

Orzech, M., F. Shi, J. Veeramony, S. Bateman, J. Calantoni, and J. Kirby, 2016: Incorporating floating surface objects into a fully dispersive surface wave model. *Ocean Mod*., 102, 14–26.

Rogers, W. E., J. Thomson, H. H. Shen, M. J. Doble, P. Wadhams, and S. Cheng, 2016: Dissipation of wind waves by pancake and frazil ice in the autumn Beaufort Sea. *J. Geophys. Res. Oceans*, 121, 7991–8007, https://doi.org/10.1002/2016JC012251.

Rogers, W.E., J. Yu, & D. Wang, 2021: Incorporating dependence on ice thickness in empirical parameterizations of wave dissipation by sea ice. *NRL Tech. Rept NRL/OT/7320-21-5145*, 35 pp.

WAVEWATCH III® Development Group (WW3DG), 2019: User manual and system documentation of WAVEWATCH III® version 6.07. *Tech. Note 333*, NOAA/NWS/NCEP/MMAB, College Park, MD, USA, 320 pp. + Appendices.

Yu, J., W.E. Rogers, & D. Wang, 2019: A scaling for wave dispersion relationships in ice-covered waters. *J. Geophys. Res*., 124. https://doi.org/10.1029/2018JC014870.

7 FURTHER READING

Squire, V.A., J. P. Dugan, P. Wadhams, P. J. Rottier, andA. K. Liu, 1995: Of ocean waves and sea ice. *Annu. Rev. Fluid Mech*., 27, 115–168, https://doi.org/10.1146/annurev.fl.27.010195.000555.

Thomson, J., 2015:ONR sea state DRI cruise report, R/V Sikuliaq, fall 2015. *APL-UW Tech. Rep. SKQ201512S*, 45 pp., http://www.apl.washington.edu/project/projects/arctic_sea_state/pdfs/cruise_report.pdf.

Thomson, J., and W. E. Rogers, 2014: Swell and sea in the emerging Arctic Ocean. *Geophys. Res. Lett*., 41, 3136–3140, https://doi.org/10.1002/2014GL059983.

Thomson, J., and Coauthors, 2013: Sea state and boundary layer physics of the emerging Arctic Ocean. *APL-UW Tech. Rep. TR1306*, 59 pp.

Timco, G. W., and W. F. Weeks, 2010: A review of the engineering properties of sea ice. *Cold Reg. Sci. Technol*., 60, 107–129, https://doi.org/10.1016/j.coldregions.2009.10.003.